Tableau 3. *Principales caractéristiques structurales des phases des systèmes* Tl_2S–Sb_2S_3 et Tl_2S–SnS

$n = \frac{Tl_2S}{SnS}$ ou $\frac{Tl_2S}{Sb_2S_3}$	1/1	3/1	1/2	2/1
	$TlSbS_2$	Tl_3SbS_3	Tl_2SnS_3	Tl_4SnS_3
Arrangement structural	Bidimensionnel	Tridimensionnel	Tridimensionnel	Bidimensionnel
Activité *E* Tl^I	Faible	Faible	Forte	Forte
Coordination Tl	7	5	4	4
Activité *E* Sb^{III} ou Sn^{II}	Moyenne	Forte	Moyenne	Nulle
Coordination Sb ou Sn	4	3	4	6

(Olivier-Fourcade, Izghouti & Philippot, 1981; Jumas, Olivier-Fourcade, Philippot & Maurin, 1983) qui montrent que l'accroissement de la teneur en cation métallique tend à diminuer la coordination de l'atome d'antimoine en augmentant la covalence des liaisons. Parallèlement on observe un renforcement de l'activité stéréochimique de la paire *E* de l'atome Sb^{III}. Par contre, l'activité de paire *E* de l'atome Tl^I reste faible quelle que soit la concentration de ce cation.

Si on compare ces résultats à ceux obtenus pour les phases du système Tl_2S–SnS (Del Bucchia *et al.*, 1981, 1982) on constate des évolutions tout à fait inverses en fonction de la concentration en thallium. Nous avons résumé les principales caractéristiques des structures de ces phases dans le Tableau 3. Quand la valeur de $n = Tl_2S/SnS$ ou Tl_2S/Sb_2S_3 augmente, la dimensionnalité des arrangements structuraux croît dans les cas de l'antimoine et décroît pour l'étain. Les différences s'étendent à l'activité stéréochimique des paires *E*. Pour le thallium, elle est toujours faible dans les thioantimonates et forte dans les thiostannates. Quant à celle de Sb^{III} elle croît quand *n* augmente et inversement pour Sn^{II}.

Etant donné les résultats obtenus lors des mesures physiques sur la phase $TlSbS_2$ (semi-conducteur de largeur de bande interdite 1,7 eV et photoconducteur, Bohac *et al.*, 1974) et, de plus, la nature non-centrosymétrique de Tl_3SbS_3, l'étude approfondie de ses propriétés physiques (électronique, optique) a été entreprise.

Références

BOHAC, P., BRÖNNIMANN, E. & GAÜMANN, A. (1974). *Mater. Res. Bull.* **9**, 1033–1040.

BONDI, A. (1964). *J. Phys. Chem.* **68**, 441–451.

BOTGROS, I. V., ZBIGLI, K. R., STEPANOV, G. I., STANCHU, A. V. & CHUMAK, G. D. (1976). *Izv. Akad. Nauk SSSR, Neorg. Mater.* **12**, 1545–1548.

COPPENS, P. & HAMILTON, W. C. (1968). *DATAPH*. Brookhaven National Laboratory, Upton, NY 11973, USA.

DEL BUCCHIA, S., JUMAS, J. C., PHILIPPOT, E. & MAURIN, M. (1981). *Rev. Chim. Minér.* **18**, 224–234.

DEL BUCCHIA, S., JUMAS, J. C., PHILIPPOT, E. & MAURIN, M. (1982). *Z. Anorg. Allg. Chem.* **48**, 199–206.

HARKER, D. (1936). *J. Chem. Phys,* **4**, 381–390.

HELLNER, E. & LEINEWEBER, G. (1956). *Z. Kristallogr.* **107**, 150–154.

International Tables for X-ray Crystallography (1974). Tome IV. Birmingham: Kynoch Press.

JUMAS, J. C., OLIVIER-FOURCADE, J., PHILIPPOT, E. & MAURIN, M. (1983). *J. Solid State Chem.* **49**, 6–13.

KUTOGLU, A. (1968). *Neues Jahrb. Mineral. Monatsh.* **10**, 145–157.

OLIVER-FOURCADE, J., IZGHOUTI, L. & PHILIPPOT, E. (1981). *Rev. Chim. Minér.* **18**, 207–217.

REY, N., JUMAS, J. C., OLIVIER-FOURCADE, J. & PHILIPPOT, E. (1983). *Acta Cryst.* C**39**, 971–974.

REY, N., JUMAS, J. C., OLIVIER-FOURCADE, J. & PHILIPPOT, E. (1984). En préparation.

SHANNON, R. D. (1976). *Acta Cryst.* A**32**, 751–767.

Acta Cryst. (1984). C**40**, 1658–1662

Neutron Diffraction Study of Natrolite, $Na_2Al_2Si_3O_{10}.2H_2O$, at 20 K

BY GILBERTO ARTIOLI AND JOSEPH V. SMITH

Department of the Geophysical Sciences, The University of Chicago, Chicago, Illinois 60637, *USA*

AND ÅKE KVICK

Brookhaven National Laboratory, Upton, New York 11973, *USA*

(*Received* 5 *March* 1984; *accepted* 15 *May* 1984)

Abstract. $M_r = 3041{\cdot}84$, orthorhombic, *Fdd*2, $a = 18{\cdot}272\ (6)$, $b = 18{\cdot}613\ (6)$, $c = 6{\cdot}593\ (2)$ Å, $V = 2242\ (2)$ Å^3, $Z = 8$, $D_x = 2{\cdot}25$ g cm^{-3}, Ge(331)-monochromatized neutrons, $\lambda = 0{\cdot}8263\ (1)$ Å, $\mu = 0{\cdot}404$ cm^{-1}, 20 K, $R(F^2) = 0{\cdot}044$ (1976 reflections). The tetrahedral sites have complete Al_2Si_3 order. Although the Si–O and Al–O distances correlate inversely with the Si–O–Al angle as for other ordered fibrous zeolites, there are differences which may relate to the ionic potential of the extraframework cations.

0108-2701/84/101658-05$01.50

© 1984 International Union of Crystallography

The hydrogen bonds follow the inverse relation between O(water)–H and O(framework)–H found in thomsonite and edingtonite.

Introduction. This fourth paper on the bonding of water molecules in fibrous zeolites [edingtonite (Kvick & Smith, 1983); scolecite (Smith, Pluth, Artioli & Ross, 1984); thomsonite (Pluth, Smith & Kvick, 1984)] provides precise coordinates for natrolite at 20 K. Positions of framework atoms, sodium atoms and water atoms at room temperature were determined with lower precision by Taylor, Meek & Jackson (1933), Meier (1960) and Torrie, Brown & Petch (1964). Most natrolite crystals are almost pure $Na_2Al_2Si_3O_{10}.2H_2O$ with essentially complete Al_2Si_3 ordering (Alberti, Pongiluppi & Vezzalini, 1982), but some have minor Al, Si disorder (Pabst, 1971; Alberti & Vezzalini, 1981; Hesse, 1983). The highest symmetry of the T_5O_{10} tetrahedral framework of natrolite is $I4_1/a2/m2/d$ (Smith, 1983), but the rotation of the 4–1 chains in the 0246 arrangement (Alberti & Gottardi, 1975) and the topochemistry of the Al_2Si_3 type of ordering result in space group *Fdd*2. Heating above room temperature causes loss of water, rotation of the 4–1 chains, and movement of the sodium atom (Peacor, 1973; Alberti & Vezzalini, 1983).

Experimental. Square prism (5·3 × 5·3 × 3·1 mm) with six faces from the {001} and {110} forms was cut from a crystal from Dutoitspan, South Africa (Cambridge University collection No. 193466). Electron microprobe analysis of a small fragment of the crystal from Dutoitspan confirmed that chemical composition is $Na_2Al_2Si_3O_{10}.2H_2O$; in particular, no Ca was detected at the 0·1wt% level. This confirms the usually pure Na composition of natrolites (Alberti *et al.*, 1982) and the hypothesis that zeolites with ordered framework have a relatively narrow compositional field (Alberti, 1979). Prism mounted on aluminum pin with **c** slightly off the φ axis of a four-circle diffractometer at the Brookhaven High Flux Beam Reactor. Crystal temperature held at 20 (0·5) K with closed-cycle refrigerator (Air Products and Chemicals, Inc., model CS-202 Displex) within He-filled aluminum can. Cell dimensions at 20 K determined by least-squares fit to $\sin^2\theta$ data from 32 reflections with $46 < 2\theta < 53°$. Reflection intensities measured by $\theta/2\theta$ step scans through Bragg peaks, scan interval $\Delta 2\theta = 3{\cdot}4°$ for $2\theta < 58°$ and $\Delta 2\theta = (3{\cdot}4 + 3{\cdot}06 \tan\theta)°$ for $2\theta > 58°$. Between 75 and 100 steps adjusted per scan with 7–10 steps representing background on either side. Each step counted for about 2 s until a preset number of counts was accumulated in direct-beam monitor. Reciprocal space explored for $+h$ $+k$ $+l$ for $2\theta < 120°$. Gaussian integration for 6 × 6 × 6 grid gave transmission factors between 0·76 and 0·90. Averaging of 2276 intensities out to $\sin\theta/\lambda = 1{\cdot}05$ Å^{-1} gave 2176 F_o^2 values for structure refinement: $R_{\rm int} = 0{\cdot}019$. h 0–34, k 0–35, l 0–11. Two standard reflections, intensity variation <2·8%. Refinement followed procedure for edingtonite (Kvick & Smith, 1983). Neutron scattering lengths given by Koester, Rauch, Herkens & Schroder (1981). Refinement of neutron scattering lengths for Si, Al, Na and water atoms consistent with Al/Si order and full occupancy of non-framework atoms. One scale factor, six extinction parameters, 33 positional and 70 anisotropic thermal parameters varied in final cycles of least-squares refinement. Full-matrix procedure minimized $\sum\omega[F_o^2 - (kF_c)^2]^2$; k is overall scale factor and $\omega^{-1} = \sigma_c^2(F_o^2) + (0{\cdot}02\, F_o^2)^2$. Extinction effects corrected using Becker & Coppens (1974, 1975) formalism assuming anisotropic type I model with Lorentzian mosaic-spread distribution. This model was significantly better than an isotropic type I or anisotropic type II model. Primary extinction may be significant for type-I-dominated extinction, and the present formalism is unreliable here for large corrections (Becker, 1977). Hence reflections with an arbitrarily chosen extinction correction larger than 1·40 were given zero weight in final cycles of refinement to avoid bias in thermal parameters. Resulting anisotropic extinction parameters are 0·118 (2), 0·248 (7), 0·071 (1), –0·041 (3), 0·072 (1), and –0·077 (3) × 10^9. Final $R(F^2) = 0{\cdot}044$ and $R_w(F^2) = 0{\cdot}059$ for 1976 reflections [$R(F^2) = 0{\cdot}054$ including 200 zero-weight reflections]. Final difference-Fourier synthesis essentially featureless with largest residual < 4% of oxygen atom. Max. $\Delta/\sigma = 0{\cdot}05$. All calculations used a crystallographic program package from the University of Uppsala (to be published).

Table 1. *Atomic coordinates and equivalent isotropic thermal parameters (expressed as average r.m.s. amplitude)*

	x	y	z	$\bar{U}$(Å)
Si(1)	0	0	0	0·058
Si(2)	0·15274 (4)	0·21171 (4)	0·62264 (19)	0·058
Al	0·03683 (4)	0·09422 (4)	0·61509 (21)	0·059
O(1)	0·02206 (3)	0·06903 (3)	0·86671 (19)	0·075
O(2)	0·06922 (3)	0·18280 (3)	0·60942 (19)	0·068
O(3)	0·09839 (3)	0·03544 (3)	0·50079 (19)	0·074
O(4)	0·20566 (3)	0·15246 (3)	0·72465 (18)	0·073
O(5)	0·17986 (3)	0·22790 (3)	0·38987 (18)	0·074
Na	0·22072 (5)	0·03063 (5)	0·61735 (22)	0·081
O*W*	0·05631 (3)	0·18948 (3)	0·11087 (19)	0·089
H(1)	0·05139 (9)	0·14423 (8)	0·03797 (31)	0·154
H(2)	0·10291 (8)	0·18912 (10)	0·17941 (34)	0·163

Discussion. The final atomic coordinates (Table 1)[*] have e.s.d.'s ten times smaller than those given by Torrie *et al.* (1964) for ordered natrolite at room temperature,

---

[*] Lists of structure factors and anisotropic thermal parameters have been deposited with the British Library Lending Division as Supplementary Publication No. SUP 39491 (24 pp.). Copies may be obtained through The Executive Secretary, International Union of Crystallography, 5 Abbey Square, Chester CH1 2HU, England.

and agree within 3σ. The small equivalent isotropic temperature factors observed at 20 K (Table 1) are consistent with the lack of substitutional disorder and the presence of only weak thermal disorder governed by atomic mass and bonding forces. The present discussion relies on the stereoview of Hesse (1983, Fig. 1).

Complete Al_2Si_3 ordering for the present natrolite was demonstrated by the refinement of scattering lengths, and is confirmed by the large value (0·34 Å) of $b - a$ which depends on the degree of ordering and associated rotation of the 4–1 chains (Alberti & Vezzalini, 1981). The inverse correlation of Al—O and Si—O distances with the Al—O—Si, Si—O—Al and Si—O—Si angles for natrolite and other ordered fibrous zeolites (Fig. 1) and particularly the different trends for Si—O—Al *vs* Si—O in natrolite and thomsonite provide yet another illustration of the well known rule that an Si,Al—O distance is not governed just by the Si,Al substitution (Gibbs, Meagher, Newton & Swanson, 1981). Even the mean of the four *T*—O distances in a tetrahedron is not a sufficient indicator of the Si,Al substitution, and the present values of 1·620 and 1·622 Å for mean Si—O and 1·747 Å for mean Al—O (Table 2) are different from the 1·612 and 1·751 Å assumed by Hesse (1983). Although there is some uncertainty in the degree of Si,Al order in albite, $NaAlSi_3O_8$, from Amelia, Virginia (Harlow & Brown, 1980), it is quite certain from the mean distances (1·609, 1·614, 1·616, 1·743 Å) for albite that the *T*—O distances in albite and natrolite are affected by more than the Si,Al substitution and the type of extra-framework cation.

Gibbs (1982) reviewed the progress in understanding the chemical and structural features of the bonding in aluminosilicates. The negative correlation of the *T*—O distance with the *T*—O—*T* angle is similar to that found for mordenite (Gibbs, Meagher, Smith & Pluth, 1977); it can be related to the *s* character of the bridging oxygen atom (Newton & Gibbs, 1980). However, each

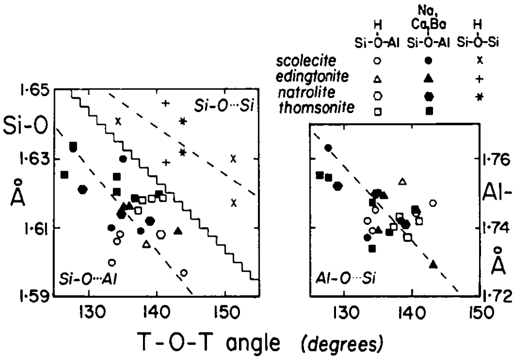

Fig. 1. Correlation between *T*—O distance and *T*—O—*T* angle for fibrous zeolites. All data are from neutron diffraction studies: scolecite (Smith *et al.*, 1984), edingtonite (Kvick & Smith, 1983), natrolite (this paper) and thomsonite (Pluth *et al.*, 1984).

Table 2. *Interatomic distances* (Å) *and angles* (°)

Si tetrahedra			
Si(1)–2O(1)	1·608 (1)	O(1)–Si(1)–O(1)	113·74 (8)
Si(1)–2O(5)	1·632 (1)	O(1)–Si(1)–O(5)	107·72 (3)
Mean	1·620 (1)	O(1)–Si(1)–O(5)	108·27 (3)
		O(5)–Si(1)–O(5)	111·17 (7)
Si(2)–O(2)	1·621 (1)	O(2)–Si(2)–O(3)	107·39 (5)
Si(2)–O(3)	1·612 (1)	O(2)–Si(2)–O(4)	111·09 (5)
Si(2)–O(4)	1·614 (1)	O(2)–Si(2)–O(5)	107·16 (5)
Si(2)–O(5)	1·641 (1)	O(3)–Si(2)–O(4)	111·79 (5)
Mean	1·622 (1)	O(3)–Si(2)–O(5)	109·75 (5)
		O(4)–Si(2)–O(5)	109·53 (5)
Al tetrahedron			
Al–O(1)	1·745 (1)	O(1)–Al–O(2)	108·99 (5)
Al–O(2)	1·752 (1)	O(1)–Al–O(3)	110·04 (5)
Al–O(3)	1·741 (1)	O(1)–Al–O(4)	112·42 (5)
Al–O(4)	1·750 (1)	O(2)–Al–O(3)	111·34 (5)
Mean	1·747 (1)	O(2)–Al–O(4)	103·99 (5)
		O(3)–Al–O(4)	109·93 (6)
T–O–*T* angles			
Si(1)–O(5)–Si(2)	144·32 (5)	Si(2)–O(3)–Al	138·92 (5)
Si(1)–O(1)–Al	140·63 (5)	Si(2)–O(4)–Al	134·79 (5)
Si(2)–O(2)–Al	129·01 (5)		
Na trigonal prism			
Na–O(2)	2·500 (1)		
Na–O(2)	2·596 (1)		
Na–O(3)	2·365 (1)		
Na–O(4)	2·391 (1)		
Na–O*W*	2·369 (1)		
Na–O*W*	2·387 (1)		
Mean	2·435 (1)		

H bonding

A–H···*B*	*A*–H*	H···*B*	*A*···*B*	∠*A*–H···*B*
O*W*–H(1)···O(1)	0·974 (2)	1·877 (2)	2·830 (1)	165·56 (16)
O*W*–H(2)···O(5)	0·964 (2)	2·103 (2)	2·999 (1)	153·82 (16)

H(1)–O*W*–H(2)	107·87 (16)
O(1)–O*W*–O(5)	134·77 (3)

* Thermal riding-motion correction increases the distances to 0·995 and 0·991 Å, respectively.

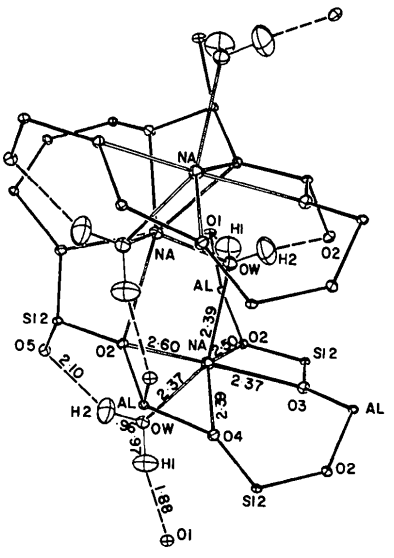

Fig. 2. Coordination of Na and H_2O. Distances in ångströms. Ellipsoids at 60% probability level.

T—O distance is also affected by the bonding to other cations and the water molecule. The longest Si—O distances are for the O(5) atom which bridges two Si and is weakly bonded to H(2) at 2·10 Å. This atom has the largest Pauling bond strength. All other oxygens are bonded to one Al and one Si, and the longest *T*—O distances are to O(2) which is bonded to two Na (at 2·50 and 2·60 Å) in contrast to O(3) and O(4) which are bonded to only one Na (at 2·36 and 2·39 Å) and O(1) which is bonded to H(1) at 1·88 Å.

The Na atom is coordinated to two water oxygens (2·37 and 2·39 Å) and four framework oxygens (Fig. 2). The coordination polyhedron is a distorted trigonal prism, whose distortion referred to the idealized shape in the notation of Muetterties & Guggenberger (1974) can be described with the dihedral angles $\delta(b_1) = 37{\cdot}61$, 35·45, 0·01; $\delta(b_2) = 132{\cdot}24$, 135·05, 149·86° and the torsional angles $\varphi = 0$, 0, 40°. Its geometrical features can be reasonably interpreted in terms of minimization of electrostatic forces. In particular, the longer distances to O(2) provide an additional compensation for the double coordination from Na. Electrostatic repulsion between Na and Al can explain the shortening of the shared edge (Pauling's third rule) between O(2) and O(4) and the small O(2)—Al—O(4) angle (104·0°).

Each water oxygen (Fig. 2) is linked to two Na at 2·37 and 2·39 Å, and the hydrogens are bonded asymmetrically to O(1) at 1·88 Å and O(5) at 2·10 Å. The tetrahedral arrangement of the two Na, H(1) and H(2) allows the Na to be bonded in the direction of the lone pairs on the water oxygen. Although the H(1)—O*W*—H(2) angle (107·9°) is larger than for water vapor (104·52°; Kuchitsu, 1971), it is close to the mean value (107·2°) calculated by Chiari & Ferraris (1982) for water in crystalline hydrates in which oxygen is the acceptor atom. Fig. 3 shows the negative correlation between O*W*—H and H···O distances for natrolite, edingtonite and thomsonite, in accordance with the results of Chiari & Ferraris (1982). As in edingtonite, O(5) in natrolite is a poor H acceptor because of saturation from bonding to two Si.

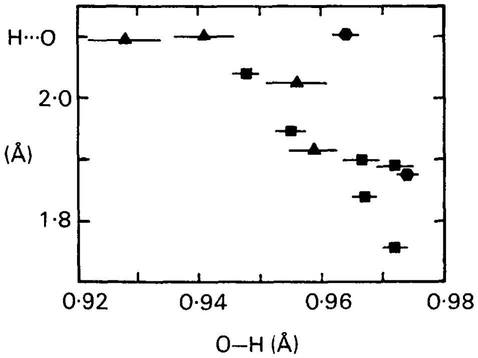

Fig. 3. Correlation between O—H and H···O distances for edingtonite (triangles), thomsonite (squares) and natrolite (hexagons). The bars across each point show ± one standard deviation.

In conclusion, the structural features of natrolite can be interpreted nicely in terms of electrostatic and electron-orbital concepts, but it must be recognized with humility that the structure is determined by an overall balance of forces which is not fully understood. The ultimate challenge is to determine why natrolite and the other fibrous zeolites are preferred in Nature to the many theoretical possibilities (Alberti & Gottardi, 1975). A neutron-diffraction refinement of natrolite at room temperature (Pechar, Schafer & Will, 1983) appeared after completion of the present study.

This research was performed at Brookhaven National Laboratory under contract OE-AC02-76 CH00016 with the US Department of Energy, Division of Chemical Sciences, Office of Basic Energy Sciences. S. O. Agrell kindly supplied the crystals of natrolite. JVS thanks NSF for grant CHE80-23444. GA is on leave of absence from Università di Modena, Italy. We thank J. Henriques, J. J. Pluth and N. Weber for technical assitance, and the following for helpful reviews: J. J. Pluth, T. F. Koetzle, R. K. McMullan and M. D. Newton.

References

Alberti, A. (1979). *Chem. Erde*, **38**, 64–82.
Alberti, A. & Gottardi, G. (1975). *Neues Jahrb. Mineral. Monatsh.* (9), 394–411.
Alberti, A., Pongiluppi, D. & Vezzalini, G. (1982). *Neues Jahrb. Mineral. Abh.* **143**, 231–248.
Alberti, A. & Vezzalini, G. (1981). *Acta Cryst.* B**37**, 781–788.
Alberti, A. & Vezzalini, G. (1983). *Neues Jahrb. Mineral. Monatsh.* (3), 135–144.
Becker, P. (1977). *Acta Cryst.* A**33**, 243–249.
Becker, P. & Coppens, P. (1974). *Acta Cryst.* A**30**, 129–153.
Becker, P. & Coppens, P. (1975). *Acta Cryst.* A**31**, 417–425.
Chiari, G. & Ferraris, G. (1982). *Acta Cryst.* B**38**, 2331–2341.
Gibbs, G. V. (1982). *Am. Mineral.* **67**, 421–450.
Gibbs, G. V., Meagher, E. P., Newton, M. D. & Swanson, D. K. (1981). *Structure and Bonding in Crystals*, edited by M. O'Keeffe & A. Navrotsky, Vol. 1, pp. 195–225. New York: Academic Press.
Gibbs, G. V., Meagher, E. P., Smith, J. V. & Pluth, J. J. (1977). *Am. Chem. Soc. Symp. Ser.* **40**, 19–29.
Harlow, G. E. & Brown, G. E. Jr (1980). *Am. Mineral.* **65**, 986–995.
Hesse, K.-F. (1983). *Z. Kristallogr.* **163**, 69–74.
Koester, L., Rauch, M., Herkens, M. & Schroder, K. (1981). KFA Report Jul-1755. Kernforschungsanlage, Jülich, Federal Republic of Germany.
Kuchitsu, K. (1971). *Bull. Chem. Soc. Jpn*, **44**, 96–99.
Kvick, Å. & Smith, J. V. (1983). *J. Chem. Phys.* **79**, 2356–2362.
Meier, W. M. (1960). *Z. Kristallogr.* **113**, 430–444.
Muetterties, E. L. & Guggenberger, L. J. (1974). *J. Am. Chem. Soc.* **96**, 1748–1756.
Newton, M. D. & Gibbs, G. V. (1980). *Phys. Chem. Miner.* **6**, 221–246.

Pabst, A. (1971). *Am. Mineral.* **56**, 560–569.
Peacor, D. R. (1973). *Am. Mineral.* **58**, 676–680.
Pechar, F., Schafer, W. & Will, G. (1983). *Z. Kristallogr.* **164**, 19–24.
Pluth, J. J., Smith, J. V. & Kvick, Å. (1984). *Zeolites*. Submitted.
Smith, J. V. (1983). *Z. Kristallogr.* **165**, 191–198.
Smith, J. V., Pluth, J. J., Artioli, G. & Ross, F. K. (1984). *Proceedings of the Sixth International Zeolite Conference.* London: Heyden.
Taylor, W. H., Meek, C. A. & Jackson, W. W. (1933). *Z. Kristallogr.* **84**, 373–398.
Torrie, B. H., Brown, I. D. & Petch, H. E. (1964). *Can. J. Phys.* **42**, 229–240.

Acta Cryst. (1984). C**40**, 1662–1665

Planar Ca–PO_4 Sheet-Type Structures: Calcium Bromide Dihydrogenphosphate Tetrahydrate, $CaBr(H_2PO_4).4H_2O$, and Calcium Iodide Dihydrogenphosphate Tetrahydrate, $CaI(H_2PO_4).4H_2O$

By M. Mathew, Shozo Takagi and W. E. Brown

American Dental Association Health Foundation Research Unit at the National Bureau of Standards, Washington, DC 20234, *USA*

(*Received* 26 *January* 1984; *accepted* 10 *May* 1984)

Abstract. $CaBr(H_2PO_4).4H_2O$ (1): $M_r = 289\cdot04$, $C2/c$, $a = 20\cdot314$ (5), $b = 6\cdot558$ (1), $c = 6\cdot973$ (1) Å, $\beta = 90\cdot02$ (2)°, $V = 928\cdot9$ (7) Å^3, $Z = 4$, $D_m = 2\cdot09$ (2), $D_x = 2\cdot066$ Mg m^{-3}, Mo $K\alpha$, $\lambda = 0\cdot7107$ Å, $\mu = 5\cdot16$ mm^{-1}, $F(000) = 576$, $T = 298$ K, $R = 0\cdot034$, 592 unique observed reflections. $CaI(H_2PO_4).4H_2O$ (2): $M_r = 336\cdot03$, $B2/c$, $a = 21\cdot416$ (4), $b = 6\cdot550$ (1), $c = 7\cdot000$ (1) Å, $\beta = 91\cdot03$ (2)°, $V = 981\cdot7$ (6) Å^3, $Z = 4$, $D_m = 2\cdot28$ (2), $D_x = 2\cdot273$ Mg m^{-3}, Mo $K\alpha$, $\lambda = 0\cdot7107$ Å, $\mu = 3\cdot92$ mm^{-1}, $F(000) = 648$, $T = 298$ K, $R = 0\cdot030$, 345 unique observed reflections. Both compounds have planar sheet-type structures consisting of Ca—H_2PO_4 chains. The halide ions, X, and the water molecules are linked *via* O—H$\cdots X$ hydrogen bonds to form $X(H_2O)_6$ octahedra. These octahedral units are linked together to form a polymeric layer $[X(H_2O)_4]_n$ between the Ca—H_2PO_4 sheets.

Introduction. A number of calcium phosphates are known to have Ca—H_2PO_4 chains consisting of corrugated sheet-type structures (Dickens & Brown, 1972). This sheet-type structure is persistent despite variations in the composition of the material between the sheets. As part of a program to study the structures of calcium phosphates, we have determined the crystal structures of $CaBr(H_2PO_4).4H_2O$ (1) and $CaI(H_2PO_4).4H_2O$ (2).

Experimental. Samples prepared by adding 1 ml of 85% H_3PO_4 to 100 ml 4 mol dm^{-3} $CaBr_2$ and 100 ml 4 mol dm^{-3} CaI_2 and allowing the resultant solutions to evaporate at room temperature (Lehr, Brown, Frazier, Smith & Thrasher, 1967). D_m by flotation. Crystals of both (1) and (2) are hygroscopic and decompose slowly in air, and were therefore mounted in sealed capillary tubes for all diffraction work; Picker diffractometer, Mo $K\alpha$ radiation, graphite monochromator; θ–2θ scan technique, 0·5° min^{-1}; backgrounds counted for 20 s at each end of scan; diffractometer-controlling programs of Lenhert (1975); structures solved from three-dimensional Patterson syntheses, remaining atoms located in subsequent Fourier syntheses, H atoms from difference Fourier syntheses; refinements by full-matrix least-squares program *RFINE*4 (Finger & Prince, 1975), function minimized $\sum w(F_o - F_c)^2$, $w^{-1} = \sigma^2(F_o) + (0\cdot02F_o)^2$; scattering factors and anomalous dispersion corrections from *International Tables for X-ray Crystallography* (1974).

Compound (1). Crystal $0\cdot07 \times 0\cdot13 \times 0\cdot34$ mm, systematic absences ($h + k = 2n + 1$ for hkl and $l = 2n + 1$ for $h0l$) consistent with space group $C2/c$ or Cc and confirmed as $C2/c$ by successful solution and refinement; unit-cell dimensions from least-squares fit of 15 reflections with $37 < 2\theta < 42°$; absorption correction applied, correction factors to F_o 1·41 to 1·83, $2\theta_{\max} = 50°$; four check reflections, monitored every 25 reflections showed steady decrease in intensity by 60% of initial values; h 0–24, k 0–7, l −8–8; 821 unique reflections, 592 observed with $F_o > 3\sigma(F_o)$; H also refined; $R = 0\cdot034$, $R_w = 0\cdot030$, $S = 0\cdot88$; av. and max. Δ/σ 0·01 and 0·07, respectively; max. and min. $\Delta\rho$ 0·6 and −0·5 e Å^{-3} respectively.

Compound (2). Crystal $0\cdot03 \times 0\cdot15 \times 0\cdot27$ mm, systematic absences ($h + l = 2n + 1$ for hkl and $l = 2n + 1$ for $h0l$) consistent with space group $B2/c$, equivalent positions: $(0,0,0;\ \tfrac{1}{2},0,\tfrac{1}{2}) + x,y,z;\ \bar{x},\bar{y},\bar{z};$